



Solar irradiances measured using SPN1 radiometers

J. Badosa et al.

Solar irradiances measured using SPN1 radiometers: uncertainties and clues for development

J. Badosa¹, J. Wood², P. Blanc³, C. N. Long⁴, L. Vuilleumier⁵, D. Demengel⁶, and M. Haeffelin⁷

¹Laboratoire de Meteorologie Dynamique, Palaiseau, France

²Peak Design, Winster, England

³MINES ParisTech, PSL Research University, O.I.E. – Centre Observation, Impacts, Energie, CS 10207 rue Claude Daunesse 06904 Sophia Antipolis Cedex, France

⁴Pacific Northwest National Laboratory, Richland, WA, USA

⁵Meteoswiss, Payerne, Switzerland

⁶EDF R&D-CEREA, Chatou, France

⁷Institut Pierre Simon Laplace (IPSL), Palaiseau, France

Received: 3 June 2014 – Accepted: 14 July 2014 – Published: 6 August 2014

Correspondence to: J. Badosa (jordi.badosa@lmd.polytechnique.fr)

Published by Copernicus Publications on behalf of the European Geosciences Union.

Title Page

Abstract

Introduction

Conclusions

References

Tables

Figures



Back

Close

Full Screen / Esc

Printer-friendly Version

Interactive Discussion



Abstract

The fast development of solar radiation and energy applications, such as photovoltaic and solar thermodynamic systems, has increased the need for solar radiation measurement and monitoring, not only for the global component but also for the diffuse and direct. End users look for the best compromise between getting close to state-of-the-art measurements and keeping low capital, maintenance and operating costs. Among the existing commercial options, SPN1 is a relatively low cost solar radiometer that estimates global and diffuse solar irradiances from seven thermopile sensors under a shading mask and without moving parts.

This work presents a comprehensive study of SPN1 accuracy and sources of uncertainty, which results from laboratory experiments, numerical modeling and comparison studies between measurements from this sensor and state-of-the art instruments for six diverse sites. Several clues are provided for improving the SPN1 accuracy and agreement with state-of-the art measurements.

1 Introduction

Developments in the use of renewable solar energy have increased the need for solar radiation measurement of global horizontal irradiance (GHI), direct normal irradiance (DNI) and diffuse horizontal irradiance (DHI) to characterize the solar resource. These in-situ pyranometric measurements are essential for region or site-specific solar resource assessment, for the monitoring of solar power plants, and also for some short-term forecasting for example for electricity grid integration. Whether for solar resource assessment at a specific site, at short timescales, or for a long-term analysis of spatial and temporal variability with a network of pyranometric sensors, all these applications require reliable continuous measurements

The current state of the art measurement uses a pyrhelimeter on a solar tracker to measure DNI, and pyranometers (one shaded by a tracker-mounted ball) to measure

AMTD

7, 8149–8191, 2014

Solar irradiances measured using SPN1 radiometers

J. Badosa et al.

Title Page

Abstract

Introduction

Conclusions

References

Tables

Figures



Back

Close

Full Screen / Esc

Printer-friendly Version

Interactive Discussion



respectively the GHI and DHI. Such instruments are used for example by the Baseline Surface Radiation Network (BSRN) network (MacArthur, 2005), but incur high capital and maintenance costs and require frequent and complex human maintenance on site. Other instruments for measuring the global, diffuse and direct components are:

1. Pyranometer for GHI, and pyranometer with shade ring for DHI. DNI can be calculated from these two components. The shade ring must be regularly manually adjusted for changes in solar declination, and a correction must be applied for the shaded part of the diffuse sky (WMO, 2010).
2. Rotating shadowband irradiometers (RSI). These use a silicon photodiode detector, and a motorized rotating shading ring to measure both the GHI and DHI. Further corrections must be applied to correct for the photodiode spectral response, cosine response and thermal response to give more accurate measurements (e.g. Geuder et al., 2003).

All of these techniques require moving parts which must be kept accurately aligned, either automatically or manually, which increases the continuing maintenance cost.

The SPN1 (Wood, 1999) is a radiometer without moving parts that measures GHI and DHI total shortwave irradiance (from 400 to 2700 nm) expressed in $W m^{-2}$. It also gives a sunshine status. The manufacturer specifies an overall accuracy for both the GHI and DHI of $\pm 8\%$ ($\pm 10 W m^{-2}$) for individual readings, which is close to the “Good Quality Pyranometer” classification by WMO. Table 1 summarizes nominal SPN1 specifications as given by Delta T (2007).

SPN1 was designed with 7 thermopiles: 6 sensors placed on a hexagonal grid, 1 sensor at the center, under a complex static shading-mask, in such a way to ensure that, at any time, for any location:

- At least one sensor is always exposed to the full solar beam
- At least one sensor is always completely shaded

AMTD

7, 8149–8191, 2014

Solar irradiances measured using SPN1 radiometers

J. Badosa et al.

Title Page

Abstract

Introduction

Conclusions

References

Tables

Figures



Back

Close

Full Screen / Esc

Printer-friendly Version

Interactive Discussion



- The solid angle of the shading-mask is equal to π , thus corresponding to half the hemispherical solid angle.

Under the assumption of isotropic diffuse sky radiance, the third property related to the shading-mask implies that all sensors receive equal amounts (50%) of diffuse irradiance from the rest of the sky hemisphere.

Figure 1 shows the parts of the sky hemisphere seen by the different sensors plotted using an equiangular projection, where radial distance on the image represents zenith angle on the hemisphere (Long et al., 2010).

DHI and GHI measurements are retrieved using a simple principle. At every measuring moment, let MIN and MAX be the minimum and maximum signals measured among the 7 sensors.

For the diffuse, SPN1 processing assumes that the half of the sky that is not seen by each sensor is exactly the same as the half that they do see.

From this:

$$DHI = 2 \times MIN \quad (1)$$

$$BHI = (MAX - MIN). \quad (2)$$

$$GHI = BHI + DHI = MAX + MIN \quad (3)$$

After this, some other calibration based on linear adjustments are applied (see the details in the Supplement).

It is necessary to notice that the sensors measuring MIN and MAX will be different at different times, and this is not trackable when using the current commercial firmware as the knowledge of the SPN1's azimuthal position is not required. However, it is to be noted that this azimuthal information can be retrieved from the analysis of the individual measurements from the 7 thermopiles available through a RS232 port.

DNI is calculated afterwards from the GHI and DHI values, as follows:

$$DNI = (GHI - DHI) / \cos(SZA) \quad (4)$$

Solar irradiances measured using SPN1 radiometers

J. Badosa et al.

Title Page	
Abstract	Introduction
Conclusions	References
Tables	Figures
◀	▶
◀	▶
Back	Close
Full Screen / Esc	
Printer-friendly Version	
Interactive Discussion	



where SZA is the Solar Zenith Angle.

More detailed technical information about SPN1 is found in its User Manual (Delta-T Devices Ltd, 2007).

SPN1 first came out about 10 years ago, and since then, its use for on-site solar resource assessment or its presence in radiation measurement networks has been growing, notably for industries in the domain of solar energy. As a consequence, the number of studies using, evaluating and comparing this sensor with other available types is increasing, although the number of related scientific publications is still low. Psiloglou et al. (2013) compared GHI and DHI measurements from SPN1 sensors against classical unshaded and ring-shaded pyranometer measurements at Penteli, Greece, during Summer 2011. They stated that accuracies were easily verified for 1 min measurements of GHI, with RMSE values varying between 2.6 % and 3.6 %, whereas for the DHI radiation, the observed RMSE (10.8–17.0 %) were not compatible with stated accuracies. They proposed new uncertainty values for the diffuse component and suggested that a correction factor should be used to improve its accuracy.

Myers and Wilcox (2009) presented the results of a comparison study of several radiometers at the US National Renewable Energy Laboratory (NREL) Solar Radiation Research Laboratory (SRRL) in Golden, Colorado. They computed bias from the comparison, which were described as function of SZA. Bias between –3.7 % and –0.7 % were found for GHI, but for DHI larger bias between –13.8 % and –4.3 % were observed. Myers (2010) found SPN1 DNI measurement differences (with respect to the reference DNI) of $\pm 15\%$ to 20% , especially at DNIs below 400 W m^{-2} . At higher DNIs, above 600 W m^{-2} , useful for concentrating solar applications, the SPN1 horizontal radiometers produced DNI estimates with uncertainty comparable to a Rotating shadowband radiometer (RSR) DNI estimates ($\pm 10\%$) for both 1 min and hourly averaged data.

The present study aims to list and quantify comprehensively the uncertainty sources for the GHI, DHI and DNI measurements when using SPN1. In particular, comparisons are made with tracker based measurements (hereafter, TBM) using pyranometers for

Solar irradiances measured using SPN1 radiometers

J. Badosa et al.

Title Page

Abstract

Introduction

Conclusions

References

Tables

Figures



Back

Close

Full Screen / Esc

Printer-friendly Version

Interactive Discussion



the GHI and DHI measurements and a pyrheliometer for DNI, which represent the state of the art for these measurements. For this, SPN1 and TBM data from six sites have been considered, together with laboratory and other ancillary measurements, some of which are original to this paper as radiative measurements.

2 Materials and methods

GHI, DHI measurements and computed DNI from SPN1 sensors with concurrent TBM measurements as a reference were considered for six sites with different geographical and meteorological contexts: 4 mid-latitude sites Winster in England, NREL's Solar Radiation Research Laboratory, (Golden, Colorado, USA), SIRTA atmospheric observatory, (Palaiseau, France), MeteoSwiss Aerological station (Payerne, Switzerland) and two tropical sites (Addu Atoll, in Maldives and Roseraye in Reunion Island). DNI for the SPN1 is computed from the 1 min averages of GHI and DHI, using Eq. (4). Table 2 summarizes the "sites" geo-location, the data temporal coverage, the instruments used and data volume descriptions.

Data from days for which operation failures can be identified (either from maintenance log-books or visual inspection of the data) were removed from the study. This corresponds to 28 days in Palaiseau (22 of these were affected by time stamp drift error for SPN1 data acquisition), 4 days in Golden, and 15 days in Roseraye (due to a cyclonic episode which made TBM unavailable for security reasons).

For Payerne, the data used is part of the DNI-comparison campaign organized in the frame of the EU funded COST Action ES1002 Weather Intelligence for Renewable Energies (WIRE). Three SPN1 radiometers have been installed for this campaign together with two triplets of rotating shadow-band radiometers from different manufacturers. Available data was already partly quality controlled, in particular for DNI reference measurements, resulting in 5.6 % of data left out in the considered period for SZA < 80 (see Table 2).

Solar irradiances measured using SPN1 radiometers

J. Badosa et al.

Title Page

Abstract

Introduction

Conclusions

References

Tables

Figures



Back

Close

Full Screen / Esc

Printer-friendly Version

Interactive Discussion



Solar irradiances measured using SPN1 radiometers

J. Badosa et al.

Title Page

Abstract

Introduction

Conclusions

References

Tables

Figures

◀

▶

◀

▶

Back

Close

Full Screen / Esc

Printer-friendly Version

Interactive Discussion



All remaining data was further tested using the BSRN recommended quality control (QC) tests (Roesch et al., 2011). Three tests for GHI, DHI and DNI measurements were performed: Extremely Rare Limits (ERL) test which sets physical upper and lower limit bounds to each quantity and two consistency tests, that is, DHI/GHI (diffuse ratio) and the ratio of GHI over calculated global from DHI and DNI (GHI/GHI^* , where $GHI^* = DNI \cdot \cos(SZA) + DHI$). This latter can only be applied to TBM since independent GHI, DHI, DNI measurements are required. The percentages of data passing the tests for $SZA < 80$ are separately given for TBM and SPN1 in Table 3.

The final considered datasets for each site were built from all 1 min data for which all tests (ERL and DHI/DHI for TBM and SPN1 and GHI/GHI^* for TBM) were passed. Data was further limited to SZA lower than 80° and both GHI and DHI measurements larger than 5 W m^{-2} . Moreover, for Palaiseau, all data for solar azimuth angle (SAA) lower than 70° (early morning summer data, with $SAA = 180$ for solar noon) was removed due to direct shadow effects on SPN1 from a surrounding meteorological mast.

Cloud fraction (CF) estimations were available for 4 sites. For Palaiseau and Golden, these were taken from the images of a co-located Total Sky Imager (TSI, Yankee Environmental Systems); for Winster and Addu Atoll, the fractional sky cover (referred to as CF in this paper) was estimated by using the TBM measurements as inputs to the Long et al. (2006) algorithm.

3 Quantitative criteria for comparison

The following metrics definitions will be used in the present work to describe the absolute and relative Dispersion and Bias Errors:

$$\text{Avg} = \frac{\sum_{t=1}^N I_{\text{TBM}}}{N} \quad (5)$$

$$STDE = \sqrt{\frac{\sum_{t=1}^N (I_{SPN1} - I_{TBM} * slope)^2}{N}} \quad (6)$$

$$RMSE = \sqrt{\frac{\sum_{t=1}^N (I_{SPN1} - I_{TBM})^2}{N}} \quad (7)$$

$$rRMSE = \frac{RMSE}{Avg} 100 \quad (8)$$

$$MAE = \frac{\sum_{t=1}^N |I_{SPN1} - I_{TBM}|}{N} \quad (9)$$

$$rMAE = \frac{MAE}{Avg} 100 \quad (10)$$

$$MBE = \frac{\sum_{t=1}^N (I_{SPN1} - I_{TBM})}{N} \quad (11)$$

$$rMBE = \frac{MBE}{Avg} 100 \quad (12)$$

I represents either GHI, DHI or DNI. N is the total number of data points considered (values in Table 3); slope, represents the slope values of the linear regression shown in Fig. 2 and Table 4.

4 General SPN1 vs. tracker-based measurements agreements

4.1 Slope comparison

General SPN1 vs. TBM comparison can be seen through scatter plots in Fig. 2, where color scale accounts for the density of points in logarithmic scale. High correlations are

Title Page	
Abstract	Introduction
Conclusions	References
Tables	Figures
◀	▶
◀	▶
Back	Close
Full Screen / Esc	
Printer-friendly Version	
Interactive Discussion	



Solar irradiances measured using SPN1 radiometers

J. Badosa et al.

Title Page

Abstract

Introduction

Conclusions

References

Tables

Figures



Back

Close

Full Screen / Esc

Printer-friendly Version

Interactive Discussion



seen in all cases with regression coefficients greater than 0.99 for all cases. Slopes are computed with least-square linear fits (forced through 0, see Fig. 2 and Table 4) and range from 0.955 to 1.021 for GHI, from 0.901 to 0.976 for DHI and from 1.009 to 1.076 for DNI. Standard deviations of the errors (STDE) around the fitting line (in percentage with respect to the mean TBM value) are also shown in Fig. 2 and range 3.4 to 4.5 % for GHI, 7.4 to 9.3 % for DHI and 8.7 to 14 % for DNI.

Figure 2 and Table 4 show that DHI is systematically underestimated for all sites and, consequently, DNI is overestimated. DHI data points in Fig. 2 are more dispersed and the STDE values are double with respect to GHI; consequently, so are the STDE values for DNI. These effects are discussed in detail in Sect. 5.

Table 4 also shows the slope values found for DHI and DNI after correcting SPN1 data for the calibration slope found for the GHI (to represent an accurate on-site re-calibration). These values are < 1 for DHI and > 1 for DNI at all stations (still showing DHI underestimations from SPN1). Winster, Palaiseau, Payerne and Golden show similar DHI slope values (0.937–0.956) while these are considerably lower for Rosearye (0.922) and Addu Atoll (0.903). This may reflect the different cloud and aerosol conditions typical for these sites, as marine aerosols typically cause more scatter, and hence a larger solar aureole, than land-based aerosols (Gueymard, 2001).

Slope values for DNI after correcting SPN1 data for the GHI slope are close to 1.05 for all sites except Golden, which is lower at 1.033. This may reflect a higher proportion of clear-sky conditions, and higher altitude, at Golden reducing the aureole effects. The solar diffuse/direct partition and aureole effects will be discussed in detail in Sect. 5.2.2.

4.2 Remaining errors after linear re-calibration

In order to remove the above found systematic SPN1-TBM differences and make it easier to compare among sites, all GHI and DHI SPN1 measurements for each site were re-calibrated by dividing by the corresponding regression slopes from Fig. 2 and Table 4. SPN1 DNI was then calculated from the re-calibrated DHI and GHI (DNI =

(GHI – DHI)/cos(SZA)). The following sections are dedicated to analyze and look for explanations for the observed remaining differences.

Figure 3 shows the histograms of the remaining differences after re-calibration for the three components at the 5 sites. Table 5 collects the percentage of data falling within ± 20 , ± 40 and $\pm 60 \text{ W m}^{-2}$ in the histograms.

Results from Fig. 3 and Table 5 show that the great majority ($> 71\%$) of GHI and DHI SPN1 measurements agree with TBM within $\pm 20 \text{ W m}^{-2}$; the percentage falls for DNI with only 50% of the data. More than 96% and more than 99% of the SPN1 GHI measurements agree with TBM measurements within $\pm 40 \text{ W m}^{-2}$ and $\pm 60 \text{ W m}^{-2}$, respectively. These percentage agreement thresholds fall to 92% and 98% for DHI and 73% and 86% for DNI.

Asymmetry is seen in the shape of histograms of DNI errors in Fig. 3. Negative (underestimation) and positive (overestimation) values are related to SPN1 sky sampling for different cloudiness conditions, especially under the presence of bright clouds and their location with respect to the Sun. DNI overestimation is related to conditions with bright solar aureole (circumsolar radiation) and DNI underestimation is related to bright clouds far from the Sun position in the sky (DHI overestimation). This will be discussed in detail in next section. Then the occurrence asymmetry seen in DNI histograms in Fig. 3 is related to different occurrence of the above-mentioned conditions.

Table 6 collects the SPN1 vs. TBM metrics results for the indicators presented in Sect. 3 (Mean Absolute Error, MAE, Mean Bias Error, MBE and Root Mean Square Error, RMSE) in absolute and relative (to the mean TBM) values. Two Tables are presented: one for the case where SPN1 data is considered without applying the linear slope re-calibration factors and the other with this re-calibration applied as described above.

As expected, all error metrics get closer to 0, in particular MBE and rMBE, after applying the re-calibration factors. Relative MAE (rMAE) values after re-calibration are generally consistent among the different sites: for GHI (rMAE values are between 2.3

Solar irradiances measured using SPN1 radiometers

J. Badosa et al.

Title Page

Abstract

Introduction

Conclusions

References

Tables

Figures



Back

Close

Full Screen / Esc

Printer-friendly Version

Interactive Discussion



Solar irradiances measured using SPN1 radiometers

J. Badosa et al.

Title Page

Abstract

Introduction

Conclusions

References

Tables

Figures



Back

Close

Full Screen / Esc

Printer-friendly Version

Interactive Discussion



However, an increase in DNI SPN1-TBM differences is found for very low SZA below 15° which does not follow the laboratory measurements. This may be because for SZA $< 15^\circ$, the effective opening angle (see Sect. 5.2.3) is always large, whereas for larger SZA, the opening angle varies from large to small with SAA. This means that for very low SZA, the DNI always includes a large part of the solar aureole, whereas for larger SZA the aureole contribution is smaller when averaged over the range of SAA.

5.1.2 Detector matching, dome lensing effect, detector hopping

The operation of the SPN1 relies on close matching of all the detectors to give a smooth output over the day, as different detectors become exposed or shaded. The graphs in Fig. 5b show how the outputs from the individual detectors rise and fall throughout the day as they are exposed to or shaded from the Sun. The GHI output will follow the upper bound plus the lower bound of these measurements, and the DHI output will follow twice the lower bound (see Eq. 3). This means that there may be apparent step changes, particularly in the GHI output trace, if different detectors are mismatched. There are two identified reasons for this:

1. Dome lensing effect. Because six of the seven detectors are located away from the centre of the protective glass dome, light reaching them from a point source is bent asymmetrically as it passes through the dome. This has the effect of increasing the measured irradiance on detectors that are on the same side of the SPN1 as the light source, and reducing the measured irradiance on detectors that are on the opposite side. This effect is calculable and predictable from the known position of the sun, provided that the SPN1 orientation is known.
2. Detector mismatches. There are several other possible sources of mismatch, such as incorrect detector calibration, imperfect horizontal mounting of the diffuser, or other manufacturing variations, which may cause detector mismatches for different solar positions. These are generally not predictable in advance.

Figure 5a shows the calculated outputs for “perfect” detectors through the course of a day in Payerne in response to a uniform point source of light, taking into account the effect of dome lensing. The arrowed points show transitions between detectors on the near and far sides of the SPN1 relative to the Sun, which will result in steps in the GHI output trace at these points.

Figure 5b shows the actual detector outputs for the same day, which was cloudless. The lower bound of the detector traces (MIN values) is raised due to the small amount of diffuse radiation on this day. Close inspection shows that the upper values for the fully exposed traces (MAX values) agree well with the modelled ones. Again, small steps in the GHI output would be visible corresponding to the arrowed transitions.

The lower graph shows how the individual detector traces would look after correcting the actual outputs for the effects of dome lensing. This results in a tighter clustering of the exposed detector readings, which should reduce the variability in the GHI output trace. The main exception is the black trace (TP3, in red, marked by arrows), which now shows a higher value in the morning, and a lower value in the afternoon, than the other exposed detector traces. Our interpretation is that this diffuser is mounted with a small deviation angle with respect the horizontal, sloping down towards the East in this case.

Figure 5d shows the resulting SPN1 GHI, DHI and DNI curves for this day, for both the original and corrected individual detector readings. It can be seen that the step near 11:00 is well corrected, and that the step near 16:00 is partly removed, though there is still a step remaining here due to the asymmetric response of TP3.

The dome lensing effects are typically of the order of up to $\pm 15 \text{ W m}^{-2}$ in the horizontal irradiance readings in bright sunshine. Steps due to detector mismatch are typically of a similar size. The two effects can add together and make larger steps like those observed in Fig. 5.

Solar irradiances measured using SPN1 radiometers

J. Badosa et al.

Title Page

Abstract

Introduction

Conclusions

References

Tables

Figures



Back

Close

Full Screen / Esc

Printer-friendly Version

Interactive Discussion



Solar irradiances measured using SPN1 radiometers

J. Badosa et al.

Title Page

Abstract

Introduction

Conclusions

References

Tables

Figures



Back

Close

Full Screen / Esc

Printer-friendly Version

Interactive Discussion

**5.2 Diffuse uncertainties**

While the GHI output of the SPN1 is generally a close equivalent of a pyranometer measurement (as discussed in Sect. 4), the DHI differences are more important in terms of relative values though similar in absolute values. There are two main contributions to this:

1. The large spectral differences in diffuse light between clear blue sky and overcast conditions.
2. Non-isotropic Diffuse radiance distribution, particularly in blue-sky or bright cloudy conditions. The DHI measurement is based on the lowest of the seven detector readings, each of which sees a different 50 % sample of the sky hemisphere. In cases where more than one sensor is fully shaded from the Sun, the SPN1's algorithm will always use the sample with the lowest measured value for calculating the DHI. This results in a negative bias compared to the TBM.

These two effects are discussed in the following subsections.

5.2.1 Spectral response

The spectral response of the SPN1 falls steeply at the blue end of the spectrum, as shown in Fig. 6. In the Near Infra-Red part, SPN1 has a higher sensitivity compared to the TBM. These spectral effects can be particularly noticeable in the measurements under two conditions.

1. The DHI output under clear blue skies is typically much lower than the TBM, due to the predominantly blue weighting of the diffuse blue sky spectrum.
2. Under heavy overcast conditions both GHI and DHI outputs are low compared with the TBM (they are also approximately equal because there is no direct beam). This appears to be because the NIR part of the solar spectrum (where the SPN1 spectral response is higher) is preferentially absorbed by heavy cloud.

Solar irradiances measured using SPN1 radiometers

J. Badosa et al.

Title Page

Abstract

Introduction

Conclusions

References

Tables

Figures



Back

Close

Full Screen / Esc

Printer-friendly Version

Interactive Discussion



To isolate the effects of spectral response from any other effects, a modified SPN1 with no internal shadowmask was used on the Winster Sun-tracker, shaded by a $\pm 2.5^\circ$ shading disk (during the same period as in Table 2). The DHI measurements from this modified SPN1 compared to the TBM DHI are presented in Fig. 6 with the color code representing data sorted in 0.1 width bins with respect to the cloud fraction from 0 to 1. The dark blue points correspond to clear sky conditions, and show a low sensitivity to diffuse light from blue sky. As the cloud fraction increases (green – yellow points), the SPN1 diffuse sensitivity increases, approaching perfect agreement (1 : 1 line) for cloud fractions near 1 (red points, corresponding to cloudy sky). More precisely, fitting linear regressions for each CF shows a progressively increasing slope with CF, from 0.72 for CF = 0 to 0.93 for CF=1. There is already a simple correction for this effect implemented in the commercial SPN1 firmware, so the normal measured differences are much less than shown in this graph (as has been seen in Fig. 2 and Table 4). The firmware correction increases the measured DHI by a factor of 1.14, which corrects for typical mixed-cloud conditions.

The heavy overcast conditions can be clearly seen by selecting readings when $GHI = DHI$ (with 3% of tolerance), and plotting the percentage difference between SPN1 and TBM against global clearness index defined as the ratio of measured GHI to GHI at the top of the atmosphere (TOA). This is shown in Fig. 6b.

For very low clearness index values when the clouds are thick, the SPN1 sensitivity reduces as clearness index reduces. Note that this may also include periods when the SPN1 and TBM instrument domes are covered with water droplets which strongly absorb the NIR part of the solar spectrum. Higher values of clearness index greater than 0.3 are typical of lighter cloud, with a diffuse spectrum very similar to global.

5.2.2 Direct/diffuse partition

Considering the sky radiance, there is always a zone close to the Sun where the radiance falls away from that of the bright solar disk towards the average level of the diffuse sky. The slope of this fall-off depends largely on the aerosol and water vapour content

Solar irradiances measured using SPN1 radiometers

J. Badosa et al.

Title Page

Abstract

Introduction

Conclusions

References

Tables

Figures

◀

▶

◀

▶

Back

Close

Full Screen / Esc

Printer-friendly Version

Interactive Discussion



of the atmosphere. The cut-off point at which the radiance is counted as DNI or DHI is to some extent arbitrary, and is usually made at 2.5° away from the sun based on the recommended opening half-angle for pyrheliometers by the CIMO guide (WMO, 2010).

As mentioned above, the DNI measurement from SPN1 is derived from the difference between the highest reading of the seven thermopile detectors (MAX), that is fully exposed to the sun and the lowest reading (MIN), that is fully shaded from the sun. Where there is more than one detector exposed to the sun, the highest reading is always used. The effective aperture for this measurement changes with the relative position of the sun with respect to SPN1 shadowmask, but it is always at least $\pm 5^\circ$, which is significantly larger than a standard pyrheliometer ($\pm 2.5^\circ$) (WMO, 2010). This means that DNI measurement from SPN1 will include a larger part of the circumsolar aureole compared to standard pyrheliometers. In other words, in most cases the DHI measurement will exclude a part of the aureole energy contribution, thus leading to DHI underestimations and DNI overestimation from SPN1 when compared to a standard TBM.

Solar Aureole measurement

There are only few reported measurements of the intensity of the solar aureole with respect to the considered opening half-angle. For example, Wilbert et al. (2011, 2012) reported aureole intensity measurements for angles between 0.475° and 5° from the centre of the sun disk. To understand the aureole for larger opening half angles relevant to the SPN1, the Winster tracker was operated with an additional shaded pyranometer with a larger shading disk covering $\pm 6.5^\circ$ (referred as $\text{DHI}_{6.5}$) during the same period as the reference TBM measurements made using a 2.5° shading ball (referred as $\text{DHI}_{2.5}$ in this section). The difference between these two measurements is the circumsolar horizontal irradiance between the half angles 2.5° and 6.5° , referred to as aureole energy in this paper.

The solar aureole energy is low for both pristine clear-sky and heavy overcast conditions and it tends to be larger as aerosol load increases, which increases the amount

Solar irradiances measured using SPN1 radiometers

J. Badosa et al.

Title Page

Abstract

Introduction

Conclusions

References

Tables

Figures

◀

▶

◀

▶

Back

Close

Full Screen / Esc

Printer-friendly Version

Interactive Discussion



of forward scattering in the vicinity of the sun. It also increases for cloudy conditions when thin clouds of cirrus type are partly covering the sun or when there are surrounding broken clouds, in which case the aureole brightness can be both large and variable over short timescales. It should also be noted that the energy in the part of the aureole

5 between the edge of the solar disk at 0.266° and 2.5° will be of a similar size to that outside 2.5° .

Figure 7a shows the direct clearness index defined as the ratio of measured DNI to DNI at the Top of the Atmosphere, plotted against the aureole energy. Again, the color scale represents the cloud fraction CF. The mean aureole energy for each direct

10 clearness index bin is also plotted. This shows that for clear skies, there is little forward scattered radiation, and the aureole energy is low. As the aureole energy increases, because the forward scattering around the Sun increases, the Direct clearness index tends to reduce and CF increases. For very low clearness index (with opaque clouds obscuring the Sun), there is little remaining direct beam, and the aureole tends to re-

15 duce back to zero. Some exceptions to this are seen in Fig. 7a, with low direct clearness index but large aureole energy, coming from scattered light around the sun that passes through the clouds under anisotropic conditions. Large aureole is related to large CF while low aureole intensity can be related to all cloudy conditions.

SPN1 dependence on aureole intensity

20 Figure 7b shows the SPN1-TBM $DHI_{2.5}$ differences at Winstar as a function of the aureole energy. The Fig. shows that the DHI underestimation by SPN1 increases with solar aureole energy, with a mean relationship close to -1 W m^{-2} for each 1 W m^{-2} of aureole energy

Table 7 compares the resulting DHI linear regression slope (after calibrating for the GHI slope, as in Table 4) and standard deviation values (analogue to the ones for

25 Fig. 2) when using $DHI_{2.5}$ and $DHI_{6.5}$ over the whole measurement period at Winstar. The slope is much closer to 1 and the standard deviation is reduced by 12% for the 6.5° shading disk, showing that a large part of the differences observed with the DHI and

conditions, that is, when it is also more likely that diffuse irradiance is highly anisotropic, in particular for cloud fraction between 0.5 and 0.9.

Figure 8b shows, for Winstar, these azimuthal dependencies of DHI differences in a scatter plot with the points color scaled for measured aureole intensity as in the previous section (that is, $DHI_{2.5} - DHI_{6.5}$). As a conclusion, the strength of the periodic variation of the DHI errors with respect to the SAA also depends on the intensity of the solar aureole.

For the case of low sun aureole energy, DHI differences are close to 0 and the SAA dependency is nearly flat. As the aureole becomes brighter, DHI differences are becoming more negative (as already seen for Fig. 7). Large underestimations are observed for cases with high aureole energy (orange and red points) following the expected 60° periodic pattern.

There are similar patterns for the tropical sites, but here the main variation is with solar zenith angle.

Actually, we find that the diffuse errors are sensitive to both azimuth and zenith solar angles, and a more sophisticated analysis is presented next to grasp the full picture.

Modelling of SPN1 effective aperture

The SPN1's thermopiles and its shadowmask arrangement have been modeled in 3-D to assess the effective opening aperture of the SPN1 for different solar positions. To simplify calculations, and because the actual sample of sky seen by each sensor is always asymmetric around the sun, the size of the largest complete circle around the sun that is seen as fully exposed or fully shaded is calculated. We have called this the "first touch angle", being the point at which a circle of increasing radius around the sun first touches an edge of the SPN1 shading pattern as seen by a specific detector. This gives a lower limit on the effective aperture angle of the SPN1 for this solar position. For the diffuse measurements, these are likely to be taken from the thermopile that has the largest first-touch angle, and hence includes the smallest amount of solar aureole.

Solar irradiances measured using SPN1 radiometers

J. Badosa et al.

Title Page

Abstract

Introduction

Conclusions

References

Tables

Figures



Back

Close

Full Screen / Esc

Printer-friendly Version

Interactive Discussion



The diffuse first touch angle is therefore the value of the largest first touch angle from the group of shaded sensors for any given solar position.

The diffuse first-touch angles are plotted in Fig. 9a by color value for all possible solar positions relative to the SPN1 orientation (in polar coordinates of SZA and SAA).

The Image color map shows low angles in red, and higher angles in blue, to match the expected diffuse differences. The red/orange areas represent solar positions where the first-touch angle is as low as 5° , and the blue areas represent first-touch angles greater than 20° . From this analysis we can see that the effective aperture for the SPN1 is always more than $\pm 5^\circ$, with a maximum value of $\pm 25^\circ$. The SPN1 will therefore exclude a large part of the solar aureole from its diffuse measurement (and include it in the DNI measurement), but the amount that is excluded will vary with solar position.

In Fig. 9b the diffuse differences for Palaiseau and Golden are plotted on the same polar projection, with the first-touch angle plot rotated to match the SPN1 orientation. A correlation can be observed between the varying effective opening angle of the SPN1, and the measured diffuse differences. The plots are shown separated out according to the cloud fraction. There is a clear correlation between the larger diffuse first touch angles and the amplitude of the negative diffuse differences (blue regions match). This is obvious for all conditions, but is most strongly seen for intermediate values of cloud fraction. For sky conditions close to overcast (CF from 0.9 and 1) DHI differences show a similar pattern as for cloudless-sky conditions (CF from 0 to 0.1), with less underestimation for the former case, due to the spectral effects discussed in Fig. 6a. However, at Golden, the DHI differences pattern, which is well defined for cloudless conditions, disappears for overcast conditions.

In Fig. 10, the DHI SPN1-TBM differences are plotted against SZA and SAA for all sites using the same polar projection and including all cloud conditions. The first touch angle diagram of Fig. 9a is simplified by plotting only the isolines for 10° , and these contours are superimposed on the plots in the correct orientation. From this figure, it can be seen that the correlation is obvious for all sites. This correlation is more significant where the dataset is larger (Golden, Palaiseau and Payerne), where the

Solar irradiances measured using SPN1 radiometers

J. Badosa et al.

Title Page

Abstract

Introduction

Conclusions

References

Tables

Figures



Back

Close

Full Screen / Esc

Printer-friendly Version

Interactive Discussion



large variability of the diffuse sky in mixed cloud conditions is averaged out over time. The correlation will also depend on the cloud regime, and will be most clearly seen in conditions of either high turbidity in clear skies, or light clouds when overcast.

Modelling of these aureole effects on the direct beam may be possible, but is complicated as DNI is retrieved from two thermopile measurements (one measuring MAX and the other measuring MIN) so it combines the different aureole view from at least 2 detectors. The DNI errors of SPN1 are dominated by the dome lensing and detector mismatch effects (Sect. 5.1.2), so the aureole effects are more difficult to distinguish.

6 Conclusions

The SPN1 is proving popular for use on solar measurement sites due to its ruggedness and simplicity of operation.

We have shown that the SPN1 performance is consistent across all of the sites we have studied, and have attempted to describe the main sources of difference between the SPN1 and tracker based measurements. The most important ones are related to the DHI measurement, mainly due to spectral and sky sampling issues. This means that, when GHI and DHI are re-calibrated, MAE is around 3% or better and it is 2–3 times larger for DHI and DNI.

Understanding these differences will help inform future data analysis and correction algorithms, as well as instrument design.

7 Further work

This analysis suggests several possibilities for improving the SPN1 accuracy and agreement with tracker based measurements, which we hope to present in a future paper. The main proposed approaches to this are:

- On-site recalibration of the SPN1.

Solar irradiances measured using SPN1 radiometers

J. Badosa et al.

Title Page

Abstract

Introduction

Conclusions

References

Tables

Figures



Back

Close

Full Screen / Esc

Printer-friendly Version

Interactive Discussion



Solar irradiances measured using SPN1 radiometers

J. Badosa et al.

Title Page

Abstract

Introduction

Conclusions

References

Tables

Figures



Back

Close

Full Screen / Esc

Printer-friendly Version

Interactive Discussion



- Once SPN1 is well calibrated for GHI, testing for a simple extra factor of 1.05 for DHI, and 0.95 for DNI readings for mid-latitude sites, as a simple solution suggested by results in Table 4.
- Further correction of DHI and DNI measurements, which could be based on the diffuse ratio (SPN1 DHI/GHI, as a proxy for cloud fraction), the clearness index, or/and on estimations of solar aureole intensity (that is, the circumsolar horizontal irradiance) and cloud fraction from other measurements.
- Correction of dome lensing and detector matching errors on the DNI measurement using outputs of the individual detectors. The SPN1 orientation would be needed for that, and it could be retrieved offline from individual thermopile measurements and information about the site location.
- Correction of the DHI measurements using outputs of the individual thermopile and knowledge of SPN1 orientation, along with solar aureole and cloud fraction estimations.

8 Supplement

Additional supporting information may be found in the online version of this article:

Section S1. Three case study examples of SPN1 and TBM GHI, DHI and DNI diurnal cycle comparison for Palaiseau together with TSI images for these days. One figure illustrates each case: Fig. S1: a cloudless day with large aureole energy due to important aerosol load (AOD at 500 nm of 0.2 in the morning and increasing to 0.3 in the afternoon). This is a good example of the azimuth effect seen in Fig. 8. Figure S2: the same effect (but larger) is seen in this case caused by the presence of bright clouds around the sun. Figure S3: day with mainly broken clouds passing (and cirrus appearing at the end of the afternoon) that lead to moments with almost cloudless, sky heterogeneous radiance and nearly overcast conditions. Consequently, quite diverse DHI SPN1-TBM difference values are found, from -50 to $+50 \text{ W m}^{-2}$.

Section S2. Polar plots for GHI and DNI SPN1-TBM. Figures S4 and S5: same as Fig. 10 but for GHI and DNI SPN1-TBM differences.

Section S3. Description of other factors affecting SPN1 measurement accuracy: thermal effects (S1.1), electrical effects (S1.2), time response (S1.3) and Soiling, rain, frost, snow (S1.4). Figure S6 shows illustrations of these effects.

Section S4. Detailed description of SPN1 standard firmware calculations.

The Supplement related to this article is available online at doi:10.5194/amtd-7-8149-2014-supplement.

Acknowledgements. This work was partly undertaken under the frame of PEGASE project with the support of ADEME, EDF R&D, ENPC, Ecole Polytechnique, and CNRS. We would like to acknowledge CEREAS-EDF for providing the surface solar irradiance measurements at Roseraie and SPN1 device at Palaiseau used in this study. We also acknowledge the contribution of the Atmospheric Radiation Measurement (ARM) Program sponsored by the US Department of Energy, Office of Science, Office of Biological and Environmental Research, Climate and Environmental Sciences Division for the Addu Atol data, and NREL's Solar Radiation Research Laboratory for the Golden data. Likewise, the Payerne Baseline Surface Radiation Network station made available the data from the COST ES1002 WIRE DNI radiometer performance evaluation. Long acknowledges support from the Office of Biological and Environmental Research of the US Department of Energy as part of the Atmospheric Systems Research Program.

Finally, we would like to thank all those instrumentalists, often unrecognised, who provide horizontal mountings, accurate datalogging, and regular cleaning and maintenance of their sensors. Without their care much of this data would be far less useful.

Solar irradiances measured using SPN1 radiometers

J. Badosa et al.

Title Page

Abstract

Introduction

Conclusions

References

Tables

Figures



Back

Close

Full Screen / Esc

Printer-friendly Version

Interactive Discussion



References

- Delta-T Devices Ltd.: User Manual for the Sunshine Pyranometer type SPN1 UM v1, available at: <http://www.delta-t.co.uk/manual.html> (last access: 13 July 2014), 2007.
- Geuder, N., Trieb, F., Schillings, C., Meyer, R., and Quaschnig, V.: Comparison of different methods for measuring solar irradiation data, in: 3rd International Conference on Experiences with Automatic Weather Stations, 2003, 2003.
- Gueymard, C. A.: Parameterized transmittance model for direct beam and circumsolar spectral irradiance, *Sol. Energy*, 71, 325–346, 2001.
- Long, C. N., Ackerman, T. P., Gaustad, K. L., and Cole, J. N. S.: Estimation of fractional sky cover from broadband shortwave radiometer measurements, *J. Geophys. Res.*, 111, D11204, doi:10.1029/2005JD006475, 2006.
- Long, C. N., Bucholtz, A., Jonsson, H., Schmid, B., Vogelmann, A. M., and Wood, J.: A method of correcting for tilt from horizontal in downwelling shortwave irradiance measurements on moving platforms, *Open Atmospheric Science Journal*, 4, 78–87, 2010.
- McArthur, L. J. B.: World Climatic Research Programme – Baseline Surface Radiation Network (BSRN) – Operations Manual Version 2.1, 2005.
- Myers, D. R.: Comparison of direct normal irradiance derived from silicon and thermopile global hemispherical radiation detectors, paper presented at SPIE Solar Energy + Technology, International Society for Optics and Photonics, 2010.
- Myers, D. R. and Wilcox, S. M.: Relative accuracy of 1 min and daily total solar radiation data for 12 global and 4 direct beam solar radiometers, paper presented at American Solar Energy Society Annual Conference Buffalo, New York, May, 2009.
- Psiloglou, B., Lykoudis, S., and Kouvas, D.: Performance assessment of an integrated sensor for simultaneous measurements of global and diffuse radiation components at Athens area, in: *Advances in Meteorology, Climatology and Atmospheric Physics*, Springer, 259–264, 2013.
- Roesch, A., Wild, M., Ohmura, A., Dutton, E. G., Long, C. N., and Zhang, T.: Assessment of BSRN radiation records for the computation of monthly means, *Atmos. Meas. Tech.*, 4, 339–354, doi:10.5194/amt-4-339-2011, 2011.
- Wilbert, S., Reinhardt, B., DeVore, J., Röger, M., Pitz-Paal, R., and Gueymard, C.: Measurement of solar radiance profiles with the Sun and Aureole Measurement system (SAM), 17th SolarPACES Conference, 20–23 September 2011, Granada, Spain, 2011.

Solar irradiances measured using SPN1 radiometers

J. Badosa et al.

Title Page

Abstract

Introduction

Conclusions

References

Tables

Figures



Back

Close

Full Screen / Esc

Printer-friendly Version

Interactive Discussion



Solar irradiances measured using SPN1 radiometers

J. Badosa et al.

Title Page

Abstract

Introduction

Conclusions

References

Tables

Figures



Back

Close

Full Screen / Esc

Printer-friendly Version

Interactive Discussion



- Wilbert, S., Pitz-Paal, R., and Jaus, J.: Circumsolar Radiation and Beam Irradiance Measurements for Focusing Collectors, COST ES1002 WIRE Workshop on “Remote Sensing Measurements for Renewable Energy”, 22–23 May 2012, DTU Risø, DK, 2012.
- 5 Wilcox, S. and Myers, D. R.: Evaluation of Radiometers in Full-Time Use at the National Renewable Energy Laboratory Solar Radiation Research Laboratory, National Renewable Energy Laboratory, 2008.
- WMO: Measurement of radiation, in: CIMO Guide to Meteorological Instruments and Methods of Observation, 7th Edn., World Meteorological Organization, WMO-No. 8 (2010 update), Geneva, Switzerland, 157–198, 2010.
- 10 Wood, J. G.: Solar Radiation Sensor, Patent WO 99/13359, 26 pp., 1999.

Solar irradiances measured using SPN1 radiometers

J. Badosa et al.

Table 1. SPN1 nominal specifications (Delta-T, 2007).

Overall accuracy: Total (global) and diffuse radiation	$\pm 5\%$ daily integrals $\pm 5\% \pm 10 \text{ W m}^{-2}$ hourly averages $\pm 8\% \pm 10 \text{ W m}^{-2}$ individual readings
Cosine response accuracy	$\pm 2\%$ of incoming radiation over $0\text{--}90^\circ$ Zenith angle
Azimuth angle accuracy	$\pm 5\%$ over 360° rotation
Temperature coefficient	$\pm 0.02\%$ per $^\circ\text{C}$ typical
Spectral sensitivity variation	10 % typical
Non-linearity	$< 1\%$
Zero offsets	$< 3 \text{ W m}^{-2}$ for a change of 5°C h^{-1} in ambient temperature $< 3 \text{ W m}^{-2}$ dark reading

Title Page

Abstract

Introduction

Conclusions

References

Tables

Figures



Back

Close

Full Screen / Esc

Printer-friendly Version







Interactive Discussion



Solar irradiances measured using SPN1 radiometers

J. Badosa et al.

Table 2. Sites, data periods and instrumental information.

Site	Latitude/Longitude/Altitude	Data period	TBM Instruments (GHI/DHI/DNI)	Sampling/storing times	SPN1 orientation
Winster	53.142° N/1.636° W/237 m	Feb 2013–Oct 2013	K&Z CMP6/CMP6/CHP1	1 s/1 min	 81°
Palaiseau	48.712° N/2.208° E/165 m	Dec 2010–Apr 2013	K&Z CMP22/CMP22/CH1	1 s/1 min	 357°
Payerne	46.815° N/6.944° E/491 m	Jun 2012–Sep 2013	K&Z CMP22/CMP22/CHP1	1 s/1 min	 196°
Golden	39.742° N/105.18° W/1829 m	Jan 2012–Oct 2013	K&ZCM22/CM22/CH1	1 s/1 min	 297°
Addu Atoll	0.688° S/73.501° E/2 m	Sep 2011–Feb 2012	Eppley PSP/8–48/NIP	1 s/1 min	 60°
Roseraie	21.137° S/55.791° E/135 m	Jul 2012–May 2013	K&Z CMP21/CMP21/CHP1	10 s/1 min	 90°

Title Page

Abstract

Introduction

Conclusions

References

Tables

Figures



Back

Close

Full Screen / Esc

Printer-friendly Version

Interactive Discussion



AMTD

7, 8149–8191, 2014

Solar irradiances measured using SPN1 radiometers

J. Badosa et al.

Table 3. Data percentage (with respect to the initial data volume for $SZA < 80^\circ$) of data not passing BSRN quality control recommended tests v2 for GHI, DHI and DNI measurements – Extremely Rare Limits (ERL), diffuse ratio test (DHI/GHI) and the ratio of GHI over calculated global from DHI and DNI (GHI/GHI^*). The percentages of data passing the tests for $SZA < 80$ are separately given for TBM and SPN1 and the total volume of data of SPN1 and TBM concurrent good data (and having GHI and $DHI > 5 \text{ W m}^{-2}$) for each site are found in the last column.

	TBM			SPN1			<i>N</i> data Final data volume (% of initial volume)	
	% ERL (GHI/DHI/DNI)	%DHI/GHI	%GHI/GHI*	% of initial volume	% ERL (GHI/DHI/DNI)	%DHI/GHI		% of initial volume
Winster	0.027/0.056/1.9	0.14	1.0	97.0	0.054/0.044/0.078	0.002	99.8	144621 (96.8)
Palaiseau	0.0060/0.11/0.97	0.0090	0.28	98.7	0.0032/0.0012/0.65	0.0018	98.5	421458 (97.2)
Payerne	0.050/0.015/0.00	0.062	0.82	93.5	0.029/0.0039/0.00035	0.00	98.5	262185 (92.0)
Golden	0.069/0.022/0.99	0.084	0.83	98.2	0.15/0.02/0.69	0.00	99.2	404622 (97.3)
Addu Atoll	0.033/0.61/0.57	0.17	0.071	99.2	0.012/0.016/0.0037	0.00	99.9	81415 (99.2)
Roseraye	0.14/0.41/0.093	1.3	0.62	95.1	0.099/0.069/3.1	0.028	94.3	133490 (92.0)

[Title Page](#)[Abstract](#)[Introduction](#)[Conclusions](#)[References](#)[Tables](#)[Figures](#)[Back](#)[Close](#)[Full Screen / Esc](#)[Printer-friendly Version](#)[Interactive Discussion](#)

Solar irradiances measured using SPN1 radiometers

J. Badosa et al.

Table 4. GHI, DHI and DNI regression slopes from Fig. 2 comparisons together with DHI and DNI slopes found after calibrating for GHI slope.

Linear regression slopes	GHI (slope/STDE(%))	DHI (slope/STDE(%))	DNI (slope/STDE(%))	DHI after calibration for GHI slope	DNI after calibration for GHI slope
Winster	1.017/4.4	0.966/7.8	1.076/15.7	0.950	1.058
Palaiseau	0.955/4.5	0.901/9.1	1.009/12.0	0.944	1.057
Payerne	1.002/3.7	0.940/8.9	1.052/10.5	0.937	1.049
Golden	1.021/4.2	0.976/9.1	1.055/8.8	0.956	1.033
Addu Atoll	1.011/3.4	0.913/9.2	1.062/9.5	0.903	1.051
Roseraye	0.993/3.8	0.916/9.0	1.043/11.8	0.922	1.050

[Title Page](#)
[Abstract](#)
[Introduction](#)
[Conclusions](#)
[References](#)
[Tables](#)
[Figures](#)

[Back](#)
[Close](#)
[Full Screen / Esc](#)
[Printer-friendly Version](#)
[Interactive Discussion](#)


Solar irradiances measured using SPN1 radiometers

J. Badosa et al.

Table 5. Percentage of data falling within ± 20 , ± 40 and ± 60 W m⁻² in SPN1 – TBM measurement differences (three values at each cell, corresponding to GHI, DHI and DNI irradiances respectively). SPN1 values have been re-calibrated as described in Sect. 4.2.

	P20	P40	P60
Winstar	88/86/70	98/98/85	100/100/93
Palaiseau	91/85/64	98/98/83	99/100/92
Payerne	93/85/60	99/98/85	99/100/94
Golden	73/87/50	96/98/73	100/100/86
Addu Atoll	76/71/51	98/93/82	100/98/94
Roseraye	79/75/54	97/92/85	99/98/94

[Title Page](#)[Abstract](#)[Introduction](#)[Conclusions](#)[References](#)[Tables](#)[Figures](#)[Back](#)[Close](#)[Full Screen / Esc](#)[Printer-friendly Version](#)[Interactive Discussion](#)

Solar irradiances measured using SPN1 radiometers

J. Badosa et al.

Table 6. SPN1 vs. TBM comparison scores before and after slope calibration (three values at each cell, corresponding to GHI, DHI and DNI irradiances respectively).

No correction applied for SPN1 data.							
	Mean TBM ($W m^{-2}$)	MAE ($W m^{-2}$)	rMAE %	MBE ($W m^{-2}$)	rMBE %	RMSE ($W m^{-2}$)	rRMSE %
Winster	312/183/215	10/11/30	3.3/5.9/14	3.8/−7.6/30	1.2/−4.2/14	15/16/44	4.9/8.8/21
Palaiseau	318/160/281	16/18/22	4.9/11/7.8	−14/−17/14	−4.4/−11/4.8	23/24/34	7.3/15/12
Payerne	358/160/314	8.3/13/28	2.3/8/8.9	0.77/−11/27	0.21/−7/8.6	13/18/41	3.8/12/13
Golden	471/154/514	18/10/44	3.7/6.6/8.5	11/−4.6/41	2.4/−3/8	23/15/58	4.9/9.6/11
Addu Atoll	532/221/426	15/23/42	2.8/11/9.8	4.6/−22/41	0.86/−10/9.6	19/30/53	3.6/14/12
Roseraye	467/231/326	13/21/31	2.8/9.2/9.4	−2.7/−19/29	−0.58/−8.4/8.9	18/31/44	3.9/13/14
SPN1 values after re-calibration as described in Sect. 4.2.							
	Mean TBM ($W m^{-2}$)	MAE ($W m^{-2}$)	rMAE %	MBE ($W m^{-2}$)	rMBE %	RMSE ($W m^{-2}$)	rRMSE %
Winster	312/183/215	9.3/10/19	3/5.5/9.0	−1.4/−1.4/8.9	−0.44/−0.77/4.1	14/15/30	4.4/8/14
Palaiseau	318/160/281	8.8/11/22	2.8/6.7/7.8	0.31/−1.7/10	0.098/−1.1/3.6	15/16/34	4.7/10/12
Payerne	358/160/314	8.2/11/22	2.3/6.6/7	−0.023/−1.5/7.8	−0.0063/−0.97/2.5	13/15/31	3.7/9.5/9.8
Golden	471/154/514	15/10/30	3.1/6.5/5.8	1.1/−0.92/18	0.23/−0.6/3.4	19/14/42	4.1/9.3/8.1
Addu Atoll	532/221/426	14/16/25	2.6/7.2/5.8	−1.1/−3.3/4.9	−0.2/−1.5/1.1	18/22/32	3.3/10/7.6
Roseraye	467/231/326	13/15/24	2.7/6.6/7.3	0.46/−0.038/4.8	0.097/−0.016/1.5	18/23/33	3.9/9.8/10

Title Page

Abstract

Introduction

Conclusions

References

Tables

Figures

◀

▶

◀

▶

Back

Close

Full Screen / Esc

Printer-friendly Version

Interactive Discussion



Solar irradiances measured using SPN1 radiometers

J. Badosa et al.

Title Page

Abstract

Introduction

Conclusions

References

Tables

Figures



Back

Close

Full Screen / Esc

Printer-friendly Version

Interactive Discussion



Table 7. Slopes of regression line and standard deviation of the Winster TBM vs. SPN1 DHI measurements for different opening angles. Recalibration for GHI slope applied to all readings, as in Table 4.

Tracker shading disk	TBM $\pm 2.5^\circ$ disk	TBM $\pm 6.5^\circ$ disk
DHI slope	0.953	0.98
DHI STD (%)	4.3	3.8

Solar irradiances measured using SPN1 radiometers

J. Badosa et al.

Title Page

Abstract

Introduction

Conclusions

References

Tables

Figures



Back

Close

Full Screen / Esc

Printer-friendly Version

Interactive Discussion



Table 8. Glossary.

BHI	Beam Horizontal Irradiance (in W m^{-2})
CC	Correlation Coefficient
CF	Cloud Fraction (from 0 to 1)
DHI	Diffuse Horizontal Irradiance (in W m^{-2})
DHI _{2.5}	Same as DHI, that is corresponding to Sun shaded by a $\pm 2.5^\circ$ of solid angle.
DHI _{6.5}	Same as DHI but with Sun shaded by a $\pm 6.5^\circ$ of solid angle.
DNI	Direct Normal Irradiance (in W m^{-2})
GHI	Global Horizontal Irradiance (in W m^{-2})
MAX	Maximum signal measured among the 7 sensors in SPN1 for a given reading time.
MAE	Mean Absolute Error
MBE	Mean Bias Error
MIN	Minimum signal measured among the 7 sensors in SPN1 for a given reading time.
rMAE	MAE relative to the mean TBM measurement
rMBE	MBE relative to the mean TBM measurement
RMSE	Root Mean Square Error
rRMSE	RMSE relative to the mean TBM measurement
SAA	Solar Azimuth Angle (in degrees)
STDE	Standard deviation Error
SZA	Solar Zenith Angle (in degrees)
TBM	Tracker Based Measurements performed with two pyranometers (for DHI and GHI) and one pyrhelimeter (for DNI) and following the BSRN measurement recommendations (Mc Arthur, 2005).
TOA	DNI at the Top Of the Atmosphere, calculated as the solar constant corrected for Earth-Sun distance (R). $\text{TOA} = 1367/R^2$ (in W m^{-2})

Solar irradiances measured using SPN1 radiometers

J. Badosa et al.

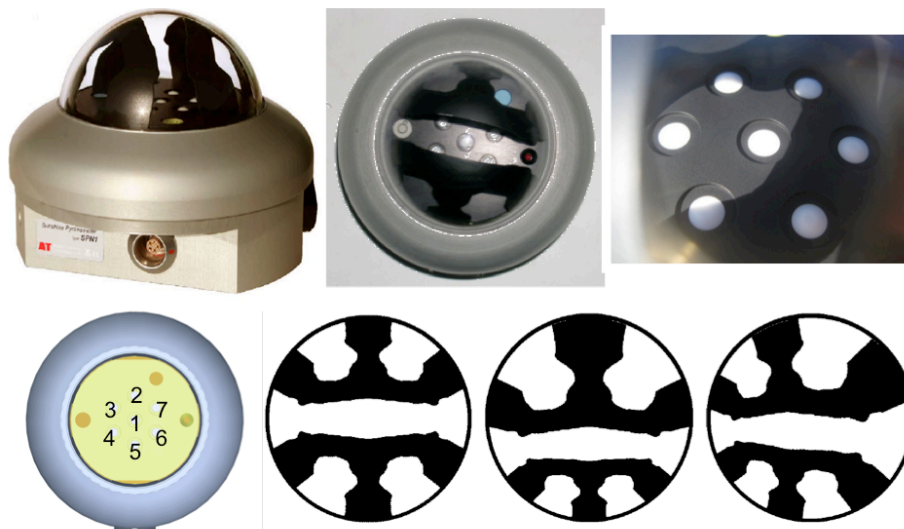


Figure 1. Top row: different SPN1 views; photo on the right shows a shadow pattern on the seven sensors for a particular sunny moment. Bottom row: SPN1 detector numbering; sky seen under shade patterns as seen for sensor 1 (left), sensors 2 and 5 (middle) and sensors 3, 4, 6, 7 (right). Sources: Long et al. (2010) and Delta T (2007).

Title Page

Abstract

Introduction

Conclusions

References

Tables

Figures

◀

▶

◀

▶

Back

Close

Full Screen / Esc

Printer-friendly Version

Interactive Discussion



Solar irradiances measured using SPN1 radiometers

J. Badosa et al.

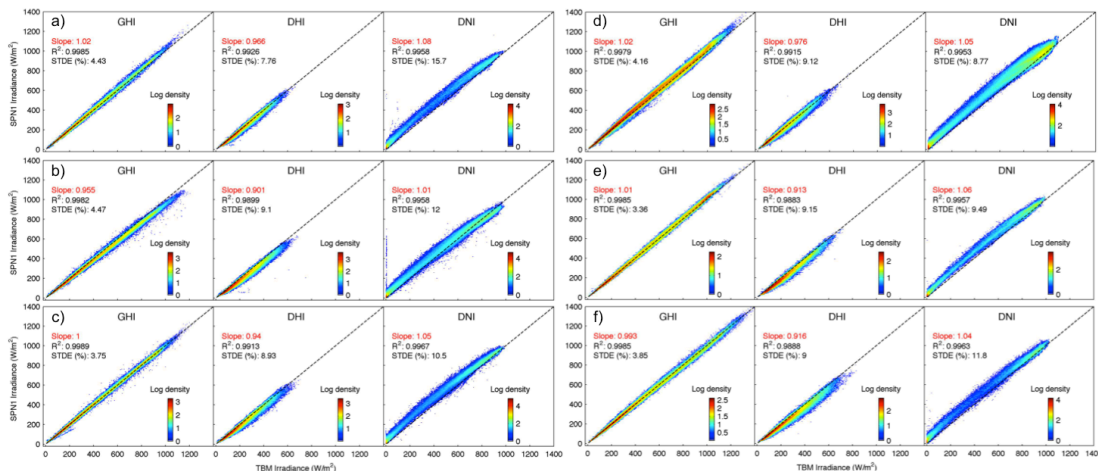


Figure 2. TBM vs. SPN1 measurements for GHI, DHI and DNI at **(a)** Winster, **(b)** Palaiseau, **(c)** Payerne, **(d)** Golden, **(e)** Addu Atoll and **(f)** Roseraye.

[Title Page](#)
[Abstract](#)
[Introduction](#)
[Conclusions](#)
[References](#)
[Tables](#)
[Figures](#)

[Back](#)
[Close](#)
[Full Screen / Esc](#)
[Printer-friendly Version](#)
[Interactive Discussion](#)


Solar irradiances measured using SPN1 radiometers

J. Badosa et al.

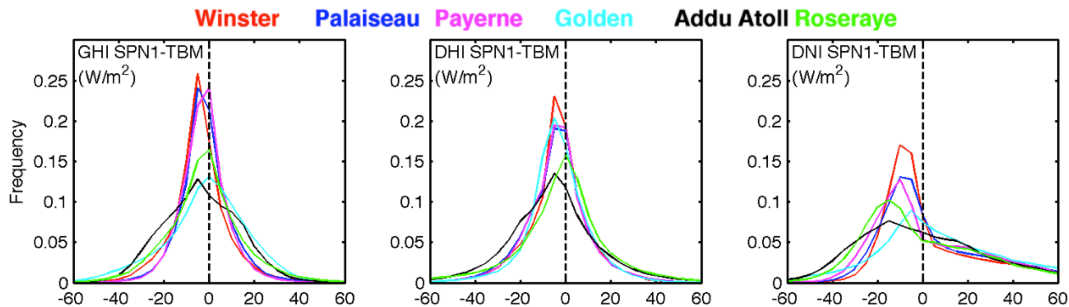


Figure 3. SPN1 – TBM difference distributions (after slope calibration) for GHI (left), DHI (center) and DNI (right) irradiance at all sites.

Title Page

Abstract

Introduction

Conclusions

References

Tables

Figures



Back

Close

Full Screen / Esc

Printer-friendly Version

Interactive Discussion



Solar irradiances measured using SPN1 radiometers

J. Badosa et al.

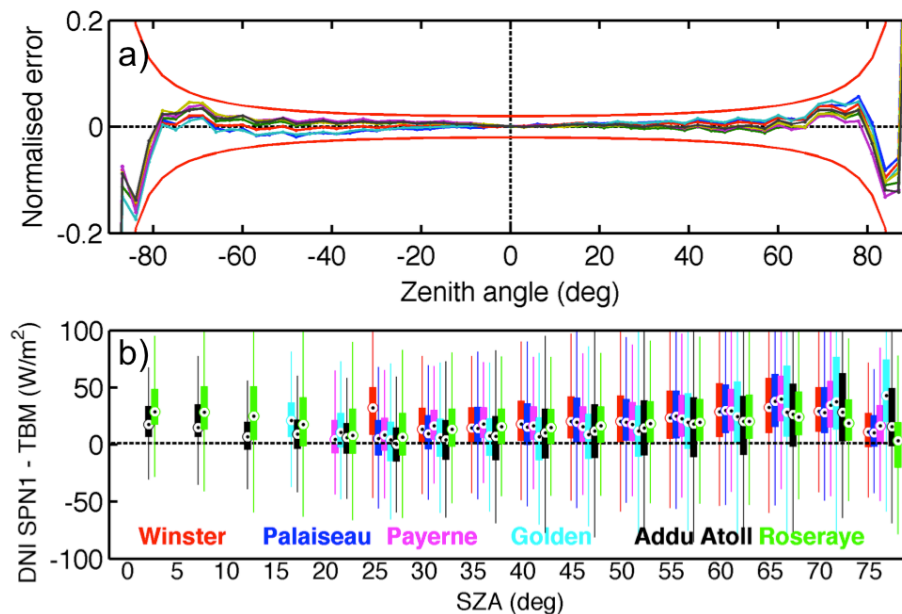


Figure 4. (a) Cosine response from laboratory tests. Shown error is normalized by incoming beam intensity. Each of thermopile readings are shown in different colors. Red envelope lines show the $\pm 2\%$ limits (from ISO 9060/1990). (b) SPN1 – TBM differences distributions for DNI, GHI and DHI as a function of bins of SZA at all stations. Box size represents the percentiles 25 and 75. Whiskers account for 99.3% of data under Gaussian distribution assumption.

Title Page

Abstract

Introduction

Conclusions

References

Tables

Figures

◀

▶

◀

▶

Back

Close

Full Screen / Esc

Printer-friendly Version

Interactive Discussion



Solar irradiances measured using SPN1 radiometers

J. Badosa et al.

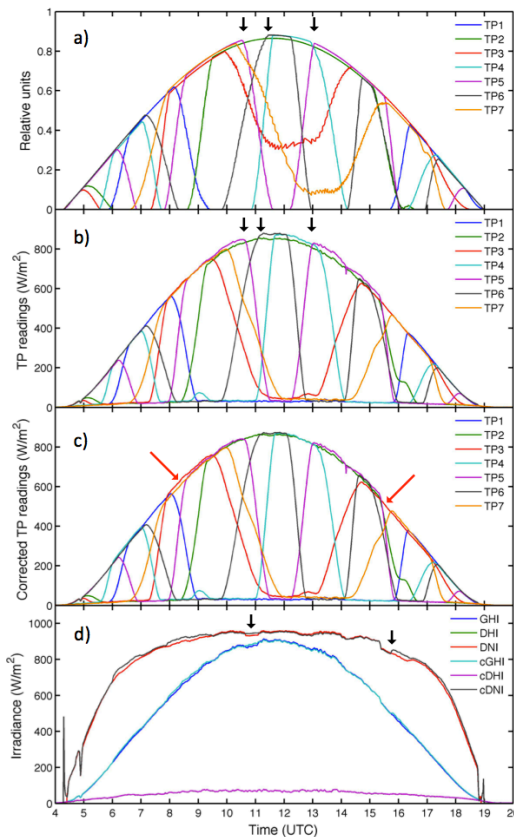


Figure 5. (a) Theoretical model of reading outputs from each of the SPN1 7 individual thermopiles (TP), theoretical model, including dome lensing, for 1 August 2013 at Payerne. (b) Actual SPN1 TP readings for this same day and place on a clear-sky day. (c) TP readings after correction for dome lensing. (d) Measured and corrected GHI, DHI and DNI measurements for this clear-sky day.

[Title Page](#)
[Abstract](#)
[Introduction](#)
[Conclusions](#)
[References](#)
[Tables](#)
[Figures](#)

[Back](#)
[Close](#)
[Full Screen / Esc](#)
[Printer-friendly Version](#)
[Interactive Discussion](#)


Solar irradiances measured using SPN1 radiometers

J. Badosa et al.

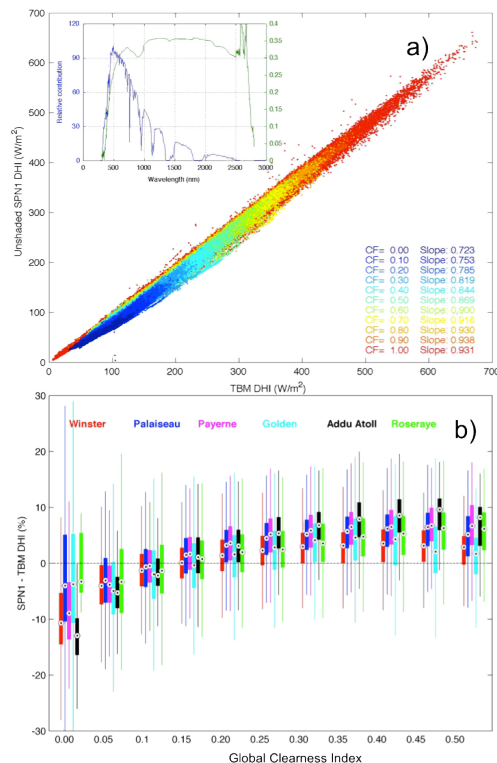


Figure 6. (a) Inner plot: standard solar spectrum (AM 1.5) and SPN1 spectral response. Main plot: SPN1 (with no internal shadowmask) DHI vs. TBM DHI sorted by cloud fraction bins (in color scale) at Winstar. The regression slope values for each bin are shown on the bottom left corner. No calibration was applied to SPN1 data. (b) DHI differences vs. clearness index in boxplots under Sun covered conditions (GHI equals DHI within 3%) at all sites. SPN1 values have been re-calibrated as described in Sect. 4.2. Box size represents the percentiles 25 and 75. Whiskers account for 99.3% of data under Gaussian distribution assumption.

Title Page

Abstract Introduction

Conclusions References

Tables Figures

◀ ▶

◀ ▶

Back Close

Full Screen / Esc

Printer-friendly Version

Interactive Discussion



Solar irradiances
measured using
SPN1 radiometers

J. Badosa et al.

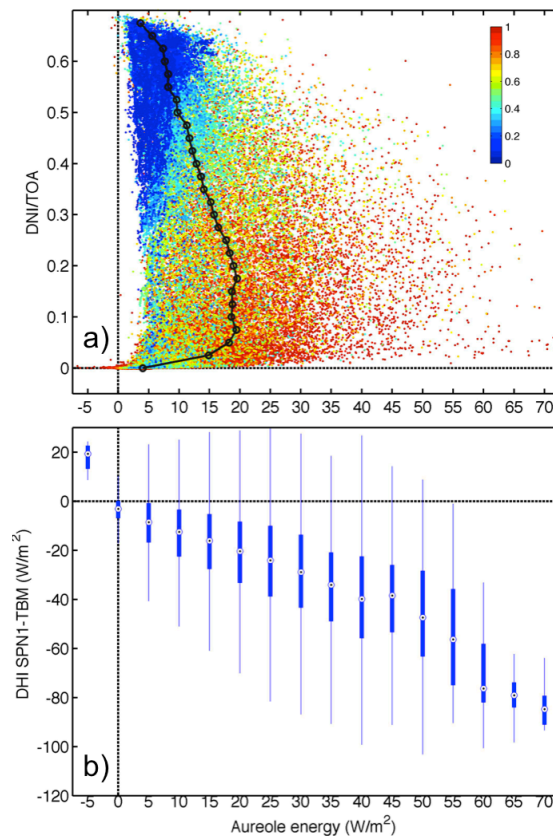


Figure 7. (a) DNI/TOA vs. aureole energy; color scale corresponds to CF (CF = 0 in blue, CF = 1 in red). Black line represents the mean aureole values for each 0.025-wide bin of DNI/TOA. (b) DHI SPN1 – TBM differences in box plots as a function of aureole energy at Winstar. Box sizes account for 25–75 percentile interval. Whisker length corresponds to approximately $\pm 2.7\sigma$ and 99.3% coverage if the data are normally distributed

Solar irradiances measured using SPN1 radiometers

J. Badosa et al.

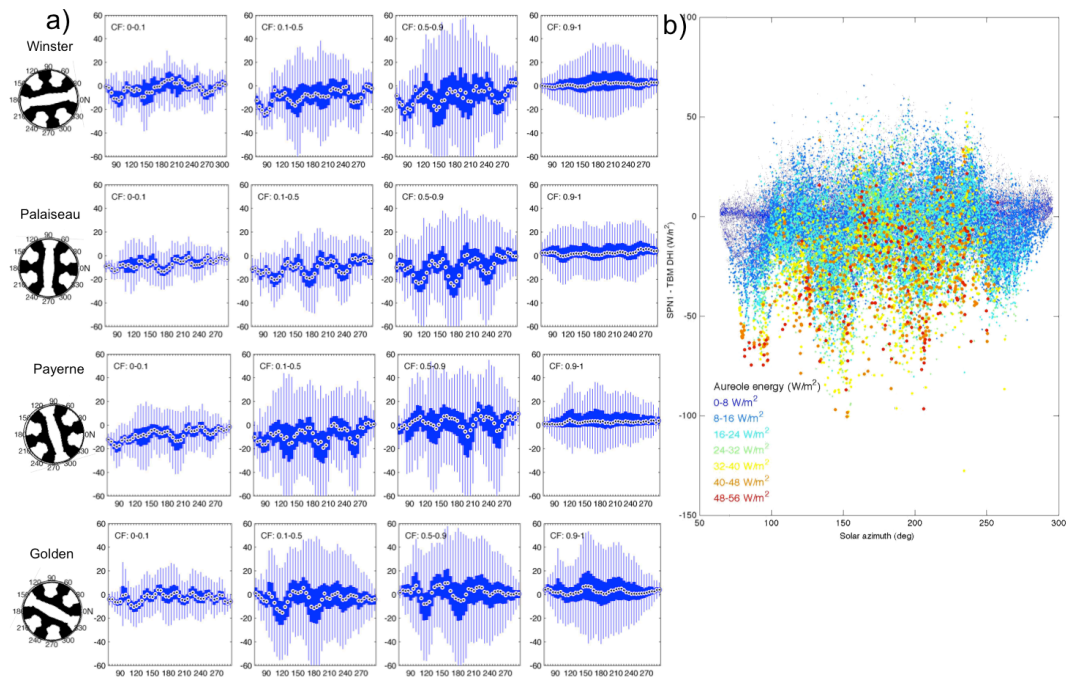


Figure 8. DHI differences (in W m^{-2}) as a function of solar azimuth angle (in degrees) and for different (a) cloud fraction values at Winster, Palaiseau, Payerne and Golden and (b) aureole intensities at Winster. The SPN1 shadowmask orientation with respect to solar azimuth ($0^\circ = \text{N}$) is shown for each site (circle drawings on the left). SPN1 values have been re-calibrated as described in Sect. 4.2.

Title Page

Abstract

Introduction

Conclusions

References

Tables

Figures

◀

▶

◀

▶

Back

Close

Full Screen / Esc

Printer-friendly Version

Interactive Discussion



Solar irradiances measured using SPN1 radiometers

J. Badosa et al.

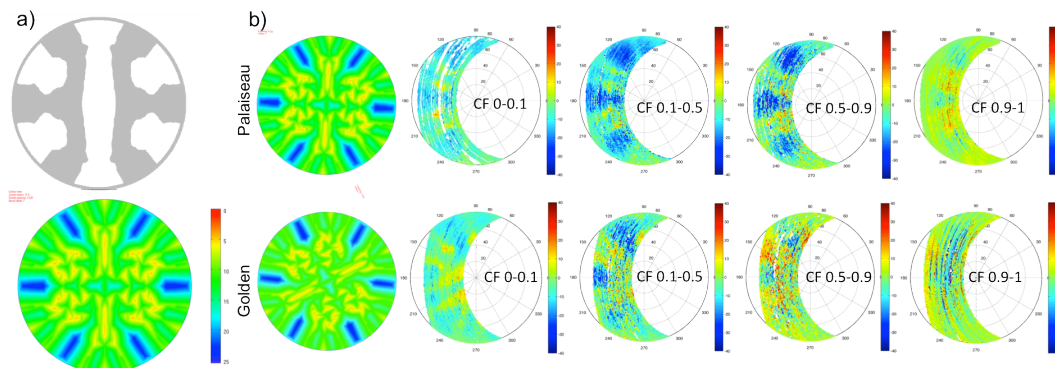


Figure 9. (a) Modelled diffuse first-touch angles for the SPN1 relative to the shadowmask. Colour scale gives angle in degrees. (b) DHI differences (TBM – SPN1) in polar coordinates (of SZA and SAA) at Palaiseau and Golden for different bins of CF with the first touch angles pattern rotated for easier visual comparison.

Title Page

Abstract

Introduction

Conclusions

References

Tables

Figures

◀

▶

◀

▶

Back

Close

Full Screen / Esc

Printer-friendly Version

Interactive Discussion



Solar irradiances measured using SPN1 radiometers

J. Badosa et al.

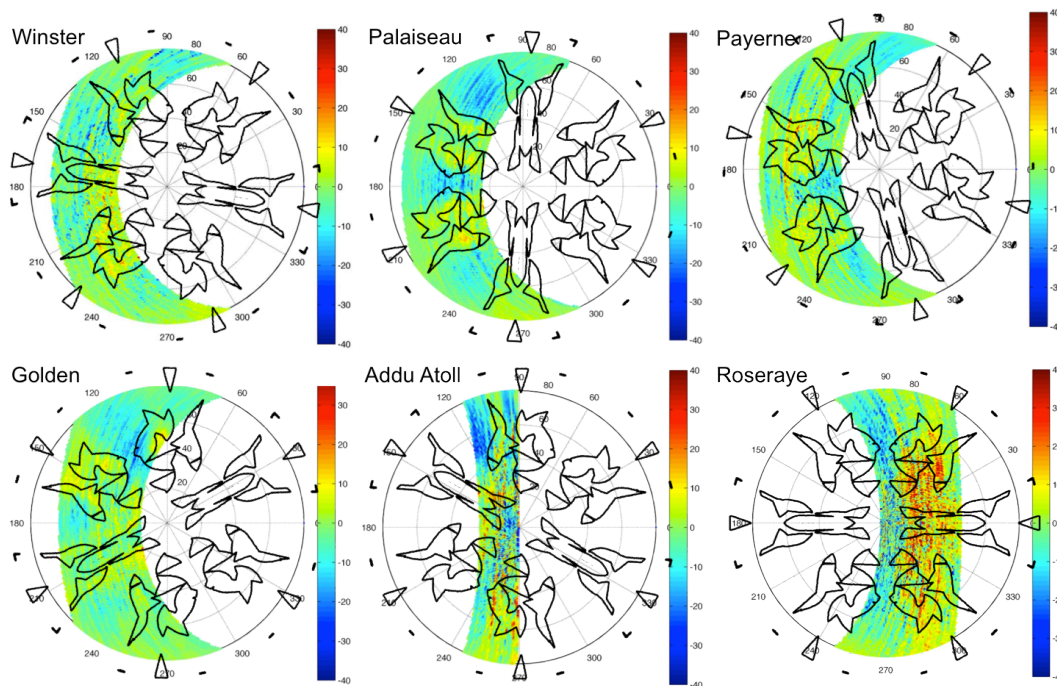


Figure 10. DHI differences (TBM – SPN1) as in Fig. 9 with the 10° first-touch-angle isolines superimposed

Title Page

Abstract

Introduction

Conclusions

References

Tables

Figures

◀

▶

◀

▶

Back

Close

Full Screen / Esc

Printer-friendly Version

Interactive Discussion

